Porous Hollow Structures

DOI: 10.1002/ange.200900539

A General Single-Source Route for the Preparation of Hollow Nanoporous Metal Oxide Structures**

Lianzhou Wang, Fengqiu Tang, Kiyoshi Ozawa, Zhi-Gang Chen, Aniruddh Mukherj, Yingchun Zhu, Jin Zou, Hui-Ming Cheng, and G. Q. (Max) Lu**

Inorganic micro- and nanosized hollow structures have attracted increasing attention in recent years because of their well-defined interior voids, low density, large surface area, stability, and surface permeability. Such materials have potential applications in a number of areas including efficient catalysts, optoelectronic sensors, drug-delivery carriers, photonic crystals, energy-storage devices, and chemical nanoreactors.[1–5] Currently, a common synthetic strategy for the fabrication of hollow structures is the utilization of various removable templates, including soft ones such as surfactants, emulsion droplets, micelles, vesicles, ionic solvents, and gas bubbles, and hard ones, such as polymers, silica, carbon, metal oxides, and metallic cores.[1–7] Recently, a few wet-chemistry template-free methods including mutual diffusion processes (known as the Kirkendall effect), galvanic replacement, and the intermediate-crystal method, have been developed by carefully tailoring the solution-based formation process of hollow microstructures.[8–16] Despite these successes, a general, economical, and scalable route to rationally fabricate hollow structures with designed internal voids, controllable shapes, and porous sizes is still a challenge and highly desirable.

Herein, we present a facile and general strategy to fabricate porous hollow microstructures by a solid-state-chemistry based controlled decomposition–dissolution (CDD) process of single metal-salt sources. The preparation of manganese oxide microboxes will be first demonstrated as an example, followed by more metal oxide examples with different compositions and nanoporous morphologies. It is demonstrated that this new strategy provides a simple template-free approach for cost-effective and scalable preparation of a wide variety of hollow structures with different compositions, variable morphologies, and tunable nanoporous structures.

Our idea was inspired by examining the thermogravimetric analysis (TGA) curve (Figure 1) of manganese carbonate cubelike microcrystals (see Experimental Section, and Supporting Information Figure S1). Thermal decomposition in air leads to the conversion of $MnCO_3$ into manganese oxide MnO_2, Mn_2O_3 or Mn_3O_4, depending upon the calcination temperature. The first steep weight loss (Figure 1, Step 1,

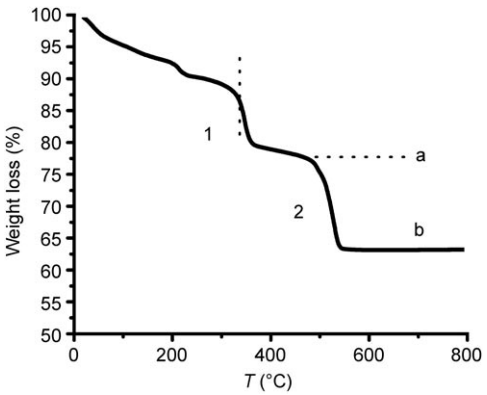

Figure 1. Thermogravimetric analysis curve of $MnCO_3$ microcubes. 1 and 2 indicate the two steep weight-loss steps; a and b indicate the two plateaus during thermal decomposition process. See text for details.

$$MnCO_3 + {}^1/_2\,O_2 \rightarrow MnO_2 + CO_2 \qquad \text{(Step1)}$$

$< 400\,°C$) is associated with the reaction of $MnCO_3$ and oxygen in air to form the MnO_2 phase and CO_2 as the byproduct, whereas the second steep weight loss (Step 2,

$$MnO_2 \rightarrow {}^1/_2\,Mn_2O_3 + {}^1/_4O_2 \qquad \text{(Step2)}$$

$< 550\,°C$) is due to the transformation of MnO_2 to Mn_2O_3 and release of O_2,[17] as depicted in the Equations describing Step 1 and Step 2.

[*] Dr. L. Z. Wang, Dr. F. Tang, A. Mukherj, Prof. G. Q. Lu
ARC Centre of Excellence for Functional Nanomaterials
School of Chemical Engineering and AIBN
The University of Queensland
St Lucia, Qld. 4072 (Australia)
E-mail: l.wang@uq.edu.au
maxlu@uq.edu.au
Dr. K. Ozawa
National Institute for Materials Science
1-2-1 Sengen, Tsukuba, Ibaraki 305-0047 (Japan)
Dr. Z.-G. Chen, Prof. H.-M. Cheng
Shenyang National Laboratory for Materials Science
Institute of Metal Research, Chinese Academy of Sciences
72 Wenhua RD, Shenyang 110016 (China)
Prof. Y. C. Zhu
The key Laboratory of Inorganic Coating Materials
Shanghai Institute of Ceramics, Chinese Academy of Sciences
1295 Dingxi RD, Shanghai 250100 (China)
Prof. J. Zou
School of Engineering and
Centre for Microscopy and Microanalysis
The University of Queensland, St Lucia, QLD, 4072 (Australia)

[**] The financial support from Australian Research Council (through its Centre's grant and DPs) is gratefully acknowledged.

Supporting information for this article is available on the WWW under http://dx.doi.org/10.1002/anie.200900539.

Commonly, to obtain the pure phase of the decomposition product as guided by the TGA curve, thermal decomposition should be conducted at a temperature of either plateau (a) (indicated by the horizontal dotted line) or (b) in Figure 1. However, if the thermal decomposition process was simply stopped at halfway, as indicated by the vertical dotted line in Figure 1, what would happen to the compound?

In this case, $MnCO_3$ can only be partially decomposed or under-calcined at this intermediate temperature, which should lead to an oxidation layer (MnO_2) on the surface of the particles, whereas the inner cores should remain as the $MnCO_3$ salt, thus forming a "core–shell" structure. The formation of this type of core–shell structure offers an excellent opportunity to further tailor the microstructure into a hollow one. Because the solubility of $MnCO_3$ ($K_{sp} \approx 10^{-11}$) is relatively large it can be easily dissolved in diluted acid, whereas MnO_2 materials are more difficult to be dissolved under the same acidic conditions. A simple acid-washing of this metal oxide/metal salt core–shell structure could easily leach out the residual $MnCO_3$ core, giving a hollow structure. Scheme 1 Steps a and b describe the proposed fabrication procedure of such hollow structures. Noting that there is a sharp weight loss in the TGA curve of $MnCO_3$ at higher temperature (Step 2 in Figure 1), which leads to crystalline shrinkage and formation unique macroporous microcubes (SEM image of Mn_2O_3 in Supporting Information, Figure S1), it is reasonable to hypothesize the formation of cagelike hollow microstructure (assuming the structure does not collapse), which arises from the shrinkage of shell framework at elevated calcination temperatures (Scheme 1, Step c). More importantly, the generality and simplicity of this strategy mean that the approach can be extended to many other material systems with different shapes including more complex ones. Scheme 1 also depicts the possible preparation of a faceted hollow particle.

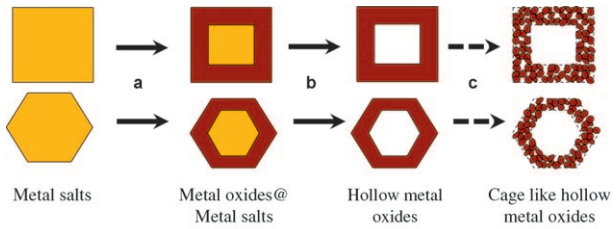

Scheme 1. The proposed controlled decomposition–dissolution method for the fabrication of nanoporous hollow structures (cross-sections only). Step a: partial thermal decomposition of metal salts (yellow) in air at an intermediate temperature, forming metal oxide outer layers (red) and leaving the cores unaffected (yellow); Step b: dissolution of the residual metal salt core, leading to hollow porous metal oxide shells; Step c: possible further calcination to form cagelike hollow structures provided further thermo-induced structural shrinkage occurs at higher temperatures.

Figure 2 provides evidence of the removal of the $MnCO_3$ core from the partially decomposed $MnCO_3$ particles by acid washing. Compared with the highly crystalline $MnCO_3$ (Figure 2A a, JCPDS Card No. 83-1763), the intensity of X-ray Diffraction (XRD) peaks is decreased considerably upon the partial decomposition of $MnCO_3$ at 350 °C for 2 h with the strongest (104) peak ($2\theta = 31.32°$) still noticeable (Figure 2A b). This process was accompanied by a color change of the material from brown to dark black. The subsequent acid washing in diluted acid (0.1 M HCl) efficiently removed the characteristic peak of $MnCO_3$. The black sample after acid washing was nearly amorphous (Figure 2A c), which could be assigned to an amorphous MnO_2 phase, as guided by the TGA curve at this temperature range. Further calcination of the acid-washed sample at higher temperatures (500 °C in this case) resulted in the formation of Mn_2O_3 phase (Figure 2A d, JCPDS Card No. 89-4836). Likewise, Fourier transform infrared spectroscopy confirmed the structure evolution during this CDD process. Two sharp vibration bands centered at 725 cm−1 and 860 cm−1, together with a broad absorbance band centered at 1410 cm−1, are the characteristic FT-IR bands of MnCO3 (Figure 2B a). Upon calcination at 350 °C, all the three vibration bands remained, whereas their intensities decreased (Figure 2B b), indicating that the $MnCO_3$ phase still exists in the sample treated at 350 °C. A noticeable change in this sample was the newly developed 515 cm^{-1} band, which can be assigned to the formation of the manganese oxide phase. Interestingly, upon acid washing of the sample treated at 350 °C, the FT-IR spectrum (Figure 2B c) showed a drastic change, with the 725 cm^{-1} and 860 cm^{-1} bands almost vanishing and significant suppression of 1410 cm^{-1} vibration. This result suggests the removal of $MnCO_3$ by the acid-washing process, and is in excellent agreement with the XRD results.

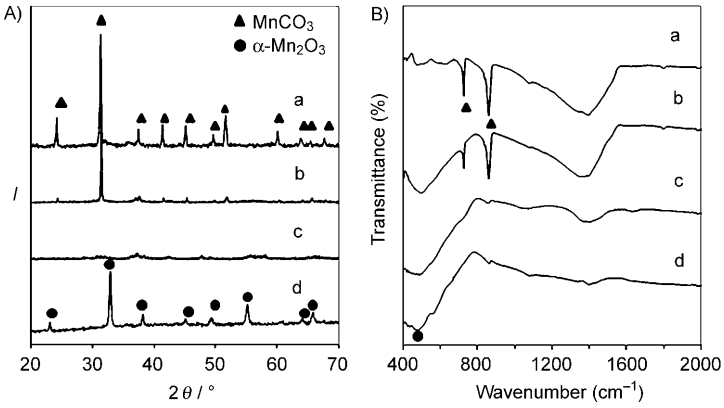

Figure 2. A) XRD patterns and B) FTIR spectra of a) as-prepared $MnCO_3$, b) the sample in (a) calcined at 350 °C for 2 h, c) the sample in (b) acid washed for 4 h, and d) the sample in (c) further calcined at 500 °C for 2 h. Symbols ▲ and ● in XRD patterns and FT-IR spectra represent the characteristic peaks (or vibration bands) of $MnCO_3$ and α-Mn_2O_3, respectively.

Figure 3 presents typical scanning electron microscopy (SEM) and transmission electron microscopy (TEM) images of the samples prepared at different stages. The as-prepared $MnCO_3$ sample had solid micrometer-sized cubelike shape, as shown in Figure 3a and b. After the CDD process, the particle morphology remained nearly intact, but some broken particles in the sample revealed a hollow box-like nature (Figure 3c). A high magnification image (Figure 3d) clearly

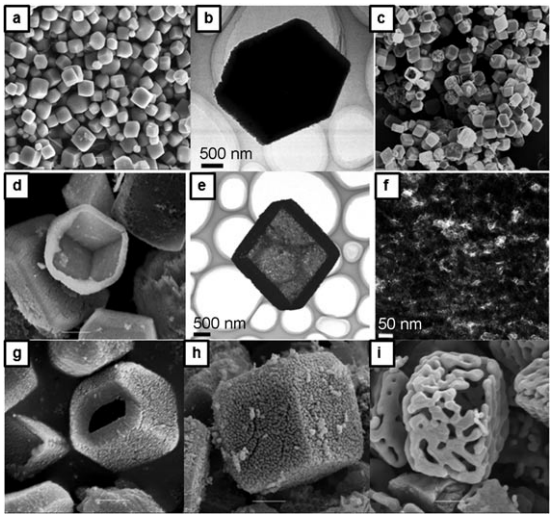

Figure 3. a) SEM and b) TEM images of the as-prepared $MnCO_3$ microcubes; c,d) SEM and e) TEM images of the acid-washed MnO_2 microboxes after calcination at 350 °C for 2 h, f) HRTEM image showing the nanoporous nature in the box framework; SEM images of g) MnO_2 boxes with thicker walls (calcined at 350 °C for 4 h, followed by acid washing) and h) Mn_2O_3 microboxes calcined at 600 °C; i) SEM image of Mn_2O_3 microcages obtained by calcination of MnO_2 microboxes at 800 °C.

shows a broken boxlike particle with dimensions of around 1.5–2 μm and wall thickness of approximately 200 nm. TEM images further support the hollow nature of the sample (Figure 3e), whereas an HRTEM image shows the box wall has a nanoporous structure (Figure 3f). The direct evidence from SEM and TEM characterizations clearly indicate that the CDD strategy is very successful. N_2 adsorption–desorption analysis revealed that the as-prepared $MnCO_3$ materials were non-porous with a very low Brunauer–Emmett–Teller (BET) specific surface area (S_{BET}) of approximately 2 $m^2 g^{-1}$; however, a porous structure with a higher S_{BET} value of 22 $m^2 g^{-1}$ was generated in the partially decomposed sample as a result of the release of CO_2 gas from the material (Supporting Information, Figure S2A). The acid-washing process further increased the nanoporosity in the material (Supporting Information, Figure S2B), resulting in a S_{BET} of 54 $m^2 g^{-1}$. This significant change in S_{BET} is attributable to the removal of the non-porous $MnCO_3$ core. The adsorption isotherm can be classified as a type IV indicating disordered mesoporous structure in the materials.

It is worth noting that the wall thickness and specific surface area of the microboxes can be easily tailored by simply controlling the calcination duration and temperature. Figure 3g shows a SEM image of the acid-washed samples after calcination at 350 °C for a longer period of time (4 h). It is clear that the wall thickness increased apparently, to around 400 nm. This effect is well understood because the further decomposition of $MnCO_3$ particles by prolonging the calcination results in thicker oxidation layers of MnO_2 on the particle surfaces. Calcination at the higher temperature of 600 °C resulted in formation of manganese oxide nanocrystallites on the wall owing to the thermal aggregation of nanoporous structures (Figure 3h). Interestingly, further increasing calcination temperature to 800 °C did not lead to the collapse of the box framework, whereas a well-defined Mn_2O_3 micro-cage structure was formed (Figure 3i), despite the significant weight loss and volume shrinkage upon heat-treatment occurring at this temperature range.[18] The boxlike shape was kept nearly intact whereas the box walls converted into an interconnected crystalline framework, with a much lower S_{BET} of less than 10 $m^2 g^{-1}$. Note that this kind of microbox may be particularly useful for chemical loading and delivery purpose because of their easily tunable size of the pores in the box walls.

To confirm the generality of our CDD strategy, transition-metal salts with different morphologies and compositions were processed (Figure 4). As expected, the hollow structures

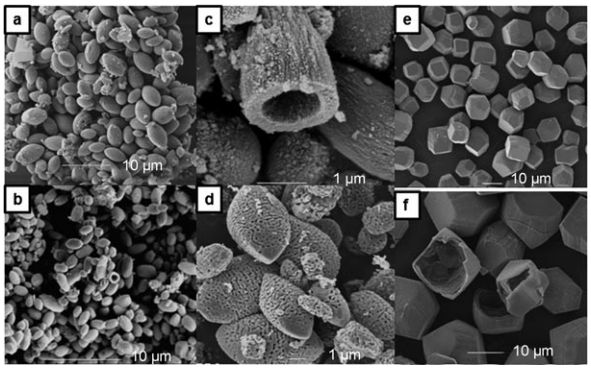

Figure 4. SEM images of a) as-prepared solid $MnCO_3$ ellipsoidal particles, b, c) acid-washed MnO_2 hollow ellipsoids after calcination at 350 °C for 2 h, d) Mn_2O_3 hollow ellipsoids calcined at 700 °C, e) as-prepared solid $FeCO_3$ faceted microparticles, and f) acid-washed Fe_2O_3 hollow particles after calcination at 300 °C for 2 h.

of manganese oxide with an ellipsoidal shape and iron oxide with more complex faceted morphologies were successfully prepared by simply adopting this strategy (Supporting Information I for experimental details, and Figures S3 and S4). This method could also be extended to commercially available chemicals. Nickel carbonate hydrate($NiCO_3 \cdot 2Ni(OH) \cdot x H_2O$) and cobalt carbonate hydrate ($CoCO_3 \cdot x H_2O$), (both of analytical grade from Aldrich without any purification), were used for this purpose. Figure 5a shows the TGA curve of nickel carbonate hydrate. When partial decomposition of the salt was conducted at an intermediate temperature (320 °C indicated by red dotted line), the light green sample changed to black (Figure 5b), whereas the acid solution after washing process provided a direct evidence of the removal of the residual cores, as demonstrated by greenish supernatant solution (dissolved Ni^{2+} salt) and black residue (nickel oxide) at the bottom of a beaker (Figure 5c). The nitrogen adsorption–desorption isotherms of the sample after acid washing exhibited higher porosity (S_{BET}: 88 $m^2 g^{-1}$; pore volume: 0.30 $cm^3 g^{-1}$), than in its counterpart before acid-washing (S_{BET}: 61 $m^2 g^{-1}$; pore volume: 0.11 $cm^3 g^{-1}$; Figure 5d). Similarly, the S_{BET} of the cobalt oxides obtained from a similar procedure was also increased noticeably (Supporting Information Figures S5, S6, and S7). Note that owing to the irregular shape of these commercial particles, it

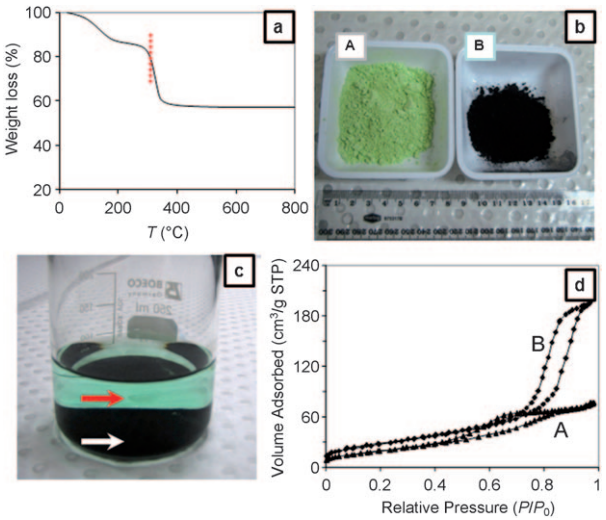

Figure 5. a) TGA curve of Aldrich nickel carbonate hydrate ($NiCO_3{\cdot}2\,Ni(OH){\cdot}x\,H_2O$); b) photo of A) the nickel carbonate hydrate and B) partially decomposed sample (320 °C). c) photo of solution after acid-washing process, with dissolved greenish nickel salt in the supernatant solution (indicated by red arrow) and the black nickel oxide residue (indicated by white arrow) at the bottom of a beaker; d) nitrogen adsorption–desorption isotherms of the A) partially calcined sample and B) the sample in (A) after acid washing.

is difficult to observe well-defined inner hollow structures; nevertheless, the nanoporous cavities in partially calcined sample was observable (Supporting Information, Figure S8).

Herein we have described a controlled decomposition–dissolution (CDD) strategy, based on a solid-state thermal decomposition process, for the preparation of nanoporous hollow structures. The approach has been demonstrated for several examples including the oxides of manganese, iron, cobalt, and nickel. Even though only metal carbonates or carbonate hydrates were used as starting salts, this method should also be applicable to other metal salt compounds, such as metal nitrates, acetates, or chlorides with different morphologies. The strategy thus can be considered as a general route to achieving a large number of nanoporous hollow structures with various compositions and morphologies. The advantages of the method lie in: a) this is a very simple single-source and cost-effective route without using any external templates or sacrificial agents; b) the composition, shape, wall thickness, and porous structure of the materials can be easily tailored by simply varying the starting metal sources and calcination conditions; and c) the procedure can be easily scaled up (10 g of sample for both nickel carbonate hydrate and cobalt carbonate hydrate), which may be particularly useful for the practical industrial applications of hollow nanoporous structures.

Experimental Section

Manganese carbonate with a microsized cubelike morphology was prepared by hydrothermal reaction of $KMnO_4$ with sucrose. In a typical experiment, $KMnO_4$ (0.632 g) was dissolved in distilled water ($20\ cm^3$) and then added to an aqueous solution ($20\ cm^3$) containing sucrose (0.5 g). The mixture was stirred for 20 min and then transferred to an autoclave ($50\ cm^3$ in volume) and hydrothermally treated at 150 °C for 24 h. The resultant precipitate was washed with copious distilled water and then was dried at 50 °C overnight to obtain the as-prepared $MnCO_3$ sample. Calcination of $MnCO_3$ was conducted in a furnace at appropriate temperatures for a certain period of time. The acid-washing process was conducted by dispersing the partially decomposed $MnCO_3$ core–shell sample (0.5 g) in HCl ($100\ cm^3$; $0.1\ mol\,dm^{-3}$) under stirring for 4 h. The resultant microbox material was collected by centrifuging the dispersion at a speed of 2000 rpm and then washed with water (3×100 ml) three times. The hollow microbox materials were further calcined at higher temperature (500–800 °C) to produce the hollow structures with different phases and porous sizes.

Received: January 29, 2009
Revised: March 23, 2009
Published online: August 24, 2009

Keywords: controlled decomposition–dissolution · nanostructures · nanoporous materials · transition metals

[1] F. Caruso, *Chem. Eur. J.* **2000**, *6*, 413.
[2] K. Kamata, Y. Lu, Y. N. Xia, *J. Am. Chem. Soc.* **2003**, *125*, 2384.
[3] C. E. Fowler, D. Khushalani, S. Mann, *Chem. Commun.* **2001**, 2028.
[4] Y. Wan, D. Y. Zhao, *Chem. Rev.* **2007**, *107*, 2821.
[5] H. Cölfen, M. Antonietti, *Angew. Chem.* **2005**, *117*, 5714; *Angew. Chem. Int. Ed.* **2005**, *44*, 5576.
[6] a) L. Z. Wang, T. Sasaki, Y. Ebina, K. Kurashima, M. Watanabe, *Chem. Mater.* **2002**, *14*, 4827; b) L. Z. Wang, Y. Ebina, K. Takada, T. Sasaki, K. Kurashima, M. Watanabe, *Chem. Commun.* **2004**, 1074; c) H. Djojoputro, X. F. Zhou, S. Z. Qiao, L. Z. Wang, C. Z. Yu, G. Q. Lu, *J. Am. Chem. Soc.* **2006**, *128*, 6320.
[7] a) D. J. Monk, D. R. Walt, *J. Am. Chem. Soc.* **2004**, *126*, 11416; b) J. Y. Gong, S. H. Yu, H. S. Qian, L. B. Luo, X. M. Liu, *Chem. Mater.* **2006**, *18*, 2012; c) X. S. Zhao, X. Y. Bao, W. P. Guo, F. Y. Lee, *Mater. Today* **2006**, *9*, 32.
[8] a) Y. Sun, Y. N. Xia, *Science* **2002**, *298*, 2176; b) Y. N. Xia, N. J. Halas, *MRS Bull.* **2005**, *30*, 338; c) Y. J. Xiong, B. Wiley, J. Y. Chen, Z. Y. Li, Y. D. Yin, Y. N. Xia, *Angew. Chem.* **2005**, *117*, 8127–8131; *Angew. Chem. Int. Ed.* **2005**, *44*, 7913–7917.
[9] H. J. Fan, U. Gosele, M. Zacharias, *Small* **2007**, *3*, 1660.
[10] a) J. J. Teo, Y. Chang, H. C. Zeng, *Langmuir* **2006**, *22*, 7369; b) H. G. Yang, H. C. Zeng, *Angew. Chem.* **2004**, *116*, 6056; *Angew. Chem. Int. Ed.* **2004**, *43*, 5930.
[11] D. Kim, J. Park, K. An, N. K. Yang, J. G. Park, T. Hyeon, *J. Am. Chem. Soc.* **2007**, *129*, 5812.
[12] Y. Liu, Y. Chu, Y. J. Zhuo, L. Dong, L. Li, M. Li, *Adv. Funct. Mater.* **2007**, *17*, 933.
[13] T. He, D. R. Chen, X. L. Jiao, Y. L. Wang, *Adv. Mater.* **2006**, *18*, 1078.
[14] X. W. Lou, C. L. Yuan, Q. Zhang, L. A. Archer, *Angew. Chem.* **2006**, *118*, 3909; *Angew. Chem. Int. Ed.* **2006**, *45*, 3825.
[15] F. H. Zhao, W. J. Lin, M. M. Wu, N. S. Xu, X. F. Yang, Z. R. Tain, Q. Su, *Inorg. Chem.* **2006**, *45*, 3356.
[16] J. B. Fei, Y. Cui, X. H. Yan, W. Qi, Y. Yang, K. W. Wang, Q. He, J. B. Li, *Adv. Mater.* **2008**, *20*, 452.
[17] W. Shaheen, M. M. M. Selim, *J. Therm. Anal. Calorim.* **2000**, *59*, 961.
[18] E. S. Toberer, R. Seshadri, *Chem. Commun.* **2006**, 3159.

